Retinal Ganglion Cell Fate Induction by Ngn-Family Transcription Factors

Ke Zhang, Wenwen Cai, Yanling Xin, Qinghai He, Canbin Chen, Mingbing Zeng, and Shuyi Chen

State Key Laboratory of Ophthalmology, Zhongshan Ophthalmic Center, Sun Yat-Sen University, Guangdong Provincial Key Laboratory of Ophthalmology and Visual Science, Guangzhou, China

Correspondence: Shuyi Chen, State Key Laboratory of Ophthalmology, Zhongshan Ophthalmic Center, Sun Yat-Sen University, Guangdong Provincial Key Laboratory of Ophthalmology and Visual Science, Guangzhou 510623, China; chenshy23@mail.sysu.edu.cn. Mingbing Zeng, State Key Laboratory of Ophthalmology, Zhongshan Ophthalmic Center, Sun Yat-Sen University, Guangdong Provincial Key Laboratory of Ophthalmology and Visual Science, Guangzhou 510623, China; zengmigb@mail.sysu.edu.cn.

KZ and WC contributed equally to this work.

Received: June 13, 2023
Accepted: November 19, 2023
Published: December 22, 2023

Citation: Zhang K, Cai W, Xin Y, et al. Retinal ganglion cell fate induction by Ngn-Family transcription factors. *Invest Ophthalmol Vis Sci.* 2023;64(15):32. https://doi.org/10.1167/iovs.64.15.32

Purpose. Retinal ganglion cells (RGCs) are the projection neurons of the retina. Loss of RGCs is the cellular basis for vision loss in patients with glaucoma. Finding ways to regenerate RGCs will aid in the development of regenerative therapies for patients with glaucoma. The aim of this study was to examine the ability of Ngn-family transcription factors (TFs) to induce RGC regeneration through reprogramming in vitro and in vivo.

Methods. In vitro, lentiviruses were used to deliver Ngn-TFs into mouse embryonic fibroblasts (MEFs). In vivo, mouse pup retina electroporation was used to deliver Ngn-TFs into late-stage retinal progenitor cells (RPCs). Immunofluorescence staining and RNA sequencing were used to examine cell fate reprogramming; patch-clamp recording was used to examine neuronal electrophysiologic functions.

Results. In vitro, all three Ngn-TFs, *Ngn1*, *Ngn2*, and *Ngn3*, were able to work alone to reprogram MEFs into RGC-like neurons that resembled RGCs at the transcriptome level, exhibited typical neuronal membrane electrophysiologic properties, and formed functional synaptic communications with retinal neurons. In vivo, Ngn-TFs reprogrammed the differentiation-competent state of late-stage RPCs to generate RGCs.

Conclusions. Ngn-TFs are effective in inducing an RGC-like fate both in vitro and in vivo and might be explored further in the future for glaucoma translational applications.

Keywords: *Ngn1*, *Ngn3*, retinal ganglion cell, reprogramming, glaucoma

Retinal ganglion cells (RGCs) are the projection neurons in the retina that are responsible for sending electrophysiologic signals generated by the visual circuits in the retina to the visual center in the brain to achieve vision. Damage to the axons of RGCs and eventual cell death are the cellular basis for glaucoma. Glaucoma, the most prevalent blinding retinal degeneration disease, is characterized by progressive peripheral-to-central visual field loss and possible eventual blindness.[1,2] Epidemiology studies estimate that approximately 3.54% of the population aged over 40 years has glaucoma, and it is predicted that the number will increase to 111.8 million in 2040.[3] Unfortunately, adult mammalian retinas cannot regenerate lost RGCs, causing the course of glaucoma to be progressive and irreversible. Developing methods to regenerate RGCs, either in vitro or in vivo, is the foundation for realizing regenerative medicine strategies to recover vision in patients with glaucoma.

Direct somatic cell reprogramming converts one type of somatic cell directly into another type of somatic cell, even a cell of a different developmental germ layer lineage. Compared to induced pluripotent stem cell strategies, direct somatic cell reprogramming provides an alternative, much simpler and faster way to generate specific somatic cells for mechanistic studies and translational applications. More intriguingly, progress has been made to reprogram somatic cells in vivo to regenerate many needed cells lost in various degenerative diseases.[4–6] In the retina, progress has also been made to explore the retinal neuron regeneration potential of Müller cells, the neural glial cells of the retina. However, the regeneration potential of Müller cells seems to be biased toward bipolar and amacrine interneurons or photoreceptors, while RGCs are rarely regenerated.[7–9] We recently developed an in vitro somatic cell direct reprogramming method that efficiently reprograms fibroblasts into RGC-like neurons by overexpressing three transcription factors (TFs), *Ascl1*, *Brn3b*, and *Islet1* (ABI). These ABI-induced RGC-like neurons resemble native RGCs at the transcriptome level and can form functional synaptic communications with native retinal bipolar interneurons.[10] Recently, the in vivo RGC-induction ability of ABI-TF combination has also been tested. The results showed signs of RGC-like fate induction from Müller cells. However, the in vivo–induced

RGC-like fate seems rudimentary, and the regenerated cells lack the typical retinal layer positioning and axon projection toward the optic nerve.[11] Thus, much effort is still needed to develop methods to regenerate RGCs.

Among the ABI-TF combination, *Ascl1* may function as the "pioneer factor" to initiate neuron fate induction, paving the way for *Brn3b* and *Islet1*, two TFs essential for the development of RGCs, to drive the induced neurons toward an RGC-like status.[10,12] However, for native RGC development in vivo, another putative pioneer factor, *Ngn2*, but not *Ascl1*, drives the RGCgenic wave in the developing retina. *Ngn2*$^+$–retinal progenitor cells (RPCs) give rise to RGCs, among other types of retinal cells, while *Ascl1*$^+$-RPCs do not produce RGCs.[13,14] *Ngn2* belongs to a three-member TF family (*Ngn1*, *Ngn2*, and *Ngn3*) that possesses potent neurogenic roles during development.[15] It has been shown that in combination with other TFs, Ngn-TFs can reprogram fibroblasts into various types of neurons.[16,17] Thus, it is worth testing the abilities of Ngn-TFs to induce RGC fate through reprogramming.

In this study, we investigated the ability of Ngn-TFs to induce RGC fate in vitro and in vivo. The results show that Ngn-TFs are able to reprogram mouse fibroblasts into functional RGC-like neurons in vitro and reprogram late-stage RPCs to change their differentiation-competent state to generate RGCs in vivo. The findings of this study emphasize the potent RGC fate induction ability of Ngn-TFs, which might be explored further in the future for glaucoma translational applications.

Methods

Cell Culture and Reprogramming

All animal studies were performed in adherence to the ARVO Statement for the Use of Animals in Ophthalmic and Vision Research. Mouse embryonic fibroblasts (MEFs) were isolated from E13.5 mouse embryos as previously described. Briefly, embryos were collected into cold PBS buffer solution. The head, spinal cord, and all internal organs were removed and the remaining tissue was cut into small pieces. The tissue was digested using TrypLE (Thermo Fisher, Waltham, MA, USA) at 37°C for 15 minutes to create a single-cell suspension. Cells were plated onto a 15-cm dish in MEF medium, consisting of Dulbecco's modified Eagle's medium (DMEM; Thermo Fisher), 10% fetal bovine serum (Biowest, Nuaillé, France), MEM nonessential amino acids (Thermo Fisher), and penicillin/streptomycin (Thermo Fisher). The cells were passaged once before being frozen for future use. To prepare lentiviruses, HEK293 cells were transfected with gene expression lentivirus plasmids, together with the two packaging plasmids, psPAX2 and pMD2.G (Addgene, Watertown, MA, USA). Thirty-six hours after transfection, viral supernatants were collected, concentrated, and frozen for future usage. For reprogramming, frozen MEFs were thawed in 24-well cell culture plates and cultured in MEF medium. On the second day after plating, the MEFs were infected with lentiviruses. Sixteen hours later, the cells were switched into fresh MEF medium plus doxycycline (2 µg/mL; Sigma-Aldrich, St. Louis, MO, USA). Forty-eight hours later, the medium was switched to neuronal medium consisting of DMEM/nutrient mixture F-12, penicillin/streptomycin, N2 (Thermo Fisher), and B27 (Thermo Fisher). Doxycycline and FGF2 were supplemented for the periods indicated in the specific parts of the Results section.

Gene Overexpression Lentivirus Plasmid Construction

The coding sequences (CDSs) of *Ngn1*, *Ngn2*, and *Ngn3* were PCR-amplified from mouse brain cDNA pools and cloned into the pSicoR-TetON vector using the restriction enzyme digestion–ligation method. To trace and sort Ngn-overexpressing cells, *pSicoR-TetON-Ngn1/2/3-ires-GFP* were constructed by adding ires-GFP after the CDSs of *pSicoR-TetON-Ngn1/2/3* using the EasyGeno Single Assembly Cloning Kit (Tiangen, Beijing, China).

Reprogramming Efficiency Calculation

Routinely, a well of MEFs infected with a specific type of virus was collected 48 hours after infection to examine the number of cells that were successfully infected. Cells were fixed and stained with specific antibodies. For *Ngn1*, an *Ngn1* antibody was used (ab66498; Abcam, Cambridge, MA, USA). For *Ngn2* and *Ngn3*, because we did not find a suitable antibody for immunostaining, *pSicoR-TetON-Ngn2/3-ires-GFP* lentiviruses were used and cells were stained with a GFP antibody (ab13970; Abcam). After staining, images were obtained with a 10× objective. Ten randomly selected 10× image fields were counted, and the number of NGN1/GFP (NGN2/3)$^+$ cells/field was averaged. Then, the total number of NGN1/GFP (NGN2/3)$^+$ cells/well was calculated based on the area relationship between the 10× image field and the entire well. At the end of reprogramming, wells were fixed and stained for TUJ1 and BRN3A. TUJ1$^+$ or BRN3A$^+$ cells were counted in a similar way as NGN1/2/3$^+$ cells at 48 hours. The reprogramming efficiency was calculated by dividing the number of TUJ1 cells by the number of NGN1/2/3$^+$ cells at 48 hours. At least three biological replicate experiments were performed, and the numbers were averaged and presented with standard deviations.

Fluorescence-Activated Cell Sorting

For fluorescence-activated cell sorting (FACS) sorting, *pSicoR-TetON-Ngn1/2/3-ires-GFP* viruses were used for reprogramming experiments. Cells were collected at either 48 hours or 14 days after infection and dissociated into single-cell suspensions using Accutase (Sigma-Aldrich). FACS was carried out on a BD FACSAria Fusion (BD Biosciences, San Jose, CA, USA).

Immunofluorescence Staining

Cells were fixed with 4% formaldehyde for 10 minutes at room temperature, washed with PBS containing 0.1% Triton X-100 (PBST), blocked with 5% normal serum (Jackson ImmunoResearch, West Grove, PA, USA) in PBST for 30 minutes, incubated with primary antibody for 2 hours at room temperature, washed with PBST three times, incubated with secondary antibody for 1 hour at room temperature, washed with PBST three times, incubated with 4′6-diamidino-2-phenylindole to stain the nuclei for 5 minutes at room temperature, and washed with PBST three times. The stained cells were observed and imaged under a ZEISS (Carl Zeiss, Jena, Germany) Axio Observer Z1inverted microscope. The antibodies used were rabbit anti-TUJ1 (802001; BioLegend, San Diego, CA, USA), mouse anti-BRN3A (MAB1585; Millipore, Merck Millipore, Billerica, MA, USA), rabbit anti-NGN1 (ab66498; Abcam), chicken anti-GFP

Investigative Ophthalmology & Visual Science

(ab13970; Abcam), rabbit anti-SYNAPSIN I (AB1543; Millipore), rabbit anti-vGLUT1 (135302; Synaptic System, Göttingen, Germany), rabbit anti-RECOVERIN (AB5585; Millipore), sheep anti-CHX10 (AB9014; Millipore), mouse HPC-1 (S0664; Sigma-Aldrich), rabbit anti-RBPMS (1830; PhosphoSolutions, Aurora, CO, USA), rabbit anti-NF200 (N4142; Sigma-Aldrich), and Alexa 488– or Alexa 568–conjugated secondary antibodies (Thermo Fisher).

Electrophysiology

Cells were grown on gelatin-coated coverslips (VWR, Radnor, PA, USA). The coverslips were placed in the recording chamber (0.5 mL in volume) on the fixed stage of an upright microscope (BX51WI; Olympus, Tokyo, Japan) equipped with epifluorescence and a 40× water-immersion objective lens. The cells were continuously perfused with oxygenated bicarbonate buffered ACSF (119 mM NaCl, 26.2 mM $NaHCO_3$, 11 mM glucose, 2.5 mM KCl, 1.0 mM K_2HPO_4, 2.5 mM $CaCl_2$, and 1.3 mM $MgCl_2$). Step current injection evoked action potentials were recorded in the current-clamp mode, with current steps at 10-pA intervals. Whole-cell currents were recorded in voltage-clamp mode with a basal holding potential of −70 mV, and voltage steps ranging from −70 to +30 mV were delivered at 10-mV increments. For spontaneous synaptic current detection, the cell membrane potential was held at −70 mV. The pipette solution for whole-cell recordings contained 120 mM potassium gluconate (130 mM CH_3O_3SCs and 5 mM QX-314 for spontaneous synaptic current), 5 mM NaCl, 10 mM KCl, 1 mM $MgCl_2$, 1 mM EGTA, 10 mM HEPES, 2 mM ATP, and 0.5 mM GTP, adjusted to pH 7.2 with 1 M KOH (CsOH for spontaneous synaptic current). Stimulus delivery and data acquisition were carried out via the HEKA EPC10 amplifier. The data were digitized at 10 kHz with a 3-kHz low-pass filter and analyzed with Patchmaster (HEKA, Frankfurt, Germany). The liquid junction potential was corrected with a value of 13.3 mV.

RNA Sequencing

Infected cells were collected 24 hours or 13 days after doxycycline induction by FACS into TRIzol (Thermo Fisher). In total, 1×10^6 cells were used for each RNA sequencing (RNA-seq) experiment. Three biological replicates were performed for each group of cells. Sequencing libraries were generated using the NEBNext Ultra RNA Library Prep Kit for Illumina (NEB, Ipswich, MA, USA). The libraries were sequenced on an Illumina HiSeq platform and 150-bp paired-end reads were generated.

RNA-Seq Data Analyses

Raw reads were filtered and trimmed to remove adapters using Trimmomatic to obtain clean reads. The clean reads were aligned to the mouse reference genome (mm10) using HISAT2. FeatureCounts was used to count the reads mapped to each gene. Differential gene expression analysis was performed using the DESeq2 R package. Genes with an adjusted P value <0.05 and fold change >2 were considered differentially expressed gene (DEGs). Gene Ontology (GO) term enrichment analysis and gene set enrichment analysis (GSEA) were performed using clusterProfiler.

Retina In Vivo Electroporation

All animal studies were performed in accordance with the protocol approved by the Institutional Animal Care and Use Committee of Zhongshan Ophthalmic Center. Retinal in vivo electroporation was performed following a published protocol.[18] Briefly, newborn mouse pups were anesthetized by chilling on ice. A small incision was made in the eyelid and sclera near the edge of the cornea with a 30-gauge needle (Hamilton, Reno, NV, USA). Purified plasmid solutions (2–5 µg/µL) in PBS were injected into the subretinal space through the previous incision using a Hamilton syringe with a 32-gauge blunt-ended needle under a dissecting microscope. After DNA injection, a tweezer-type electrode was placed to softly hold the pup heads, and five 80-V pulses of 50-ms duration and 950-ms intervals were applied using a Gemini X2 pulse generator (BTX, Hartford, MA, USA). After electroporation, the pups were allowed to recover on a warming pad until they regained consciousness and were returned to their mother. The pups were sacrificed at p14 (postnatal day 14), and the retinas were collected and subjected to cryosection. Eye sections were immunostained for GFP (to recognize transduced cells and their progenies) and SOX9 (to recognize Müller cells), RECOVERIN (to recognize photoreceptors), CHX10 (to recognize bipolar cells), and HPC-1 (to recognize amacrine cells).

Statistical Analysis

All experiments whose data were subjected to statistical analysis were performed with at least three biological replicates. Quantification data are presented as the mean ± standard deviation, and the significance of differences between samples was assessed using Student's t-test.

Results

Single Ngn Family TFs (Ngn-TFs) Are Sufficient to Induce BRN3A$^+$-Induced Neurons

To test the ability of Ngn-TFs to induce RGC-like fate through direct somatic cell reprogramming in vitro, we transfected MEFs with lentiviruses expressing *Ngn1*(*pSicoR-TetON-Ngn1*), *Ngn2*(*pSicoR-TetON-Ngn2-ires-GFP*), or *Ngn3*(*pSicoR-TetON-Ngn3-ires-GFP*) under the control of a Tet-On promoter. For comparison, we also included an experimental group overexpressing *Ascl1*(*pSicoR-TetON-Ascl1*), the pioneer TF that exhibits potent neuronal fate induction ability in many induced neuron (iN) induction systems, including our previous ABI-iRGC system.[10] We allowed the exogenous genes to be expressed for 7 days by supplementing the culture medium with doxycycline (Dox) and collected the cells 6 days after Dox withdrawal (Fig. 1A and Supplementary Fig. S1), the protocol we used previously for ABI-iRGC induction. We stained the cells for TUJ1 to recognize generic neuronal fate and BRN3A for putative RGC fate, which is strongly expressed in native RGCs and plays essential roles in RGC development in vivo.[19] In the control group with no exogenous TF added, no TUJ1$^+$ or BRN3A$^+$ cells were observed (Fig. 1B-e). In contrast, in the three experimental groups overexpressing *Ngn1*, *Ngn2*, or *Ngn3*, as well as the group overexpressing *Ascl1*, many TUJ1$^+$ cells with elaborate long cellular processes were observed, demonstrating that Ngn-TFs alone were able to induce neuron fate (iNs) from MEFs (Fig. 1B).

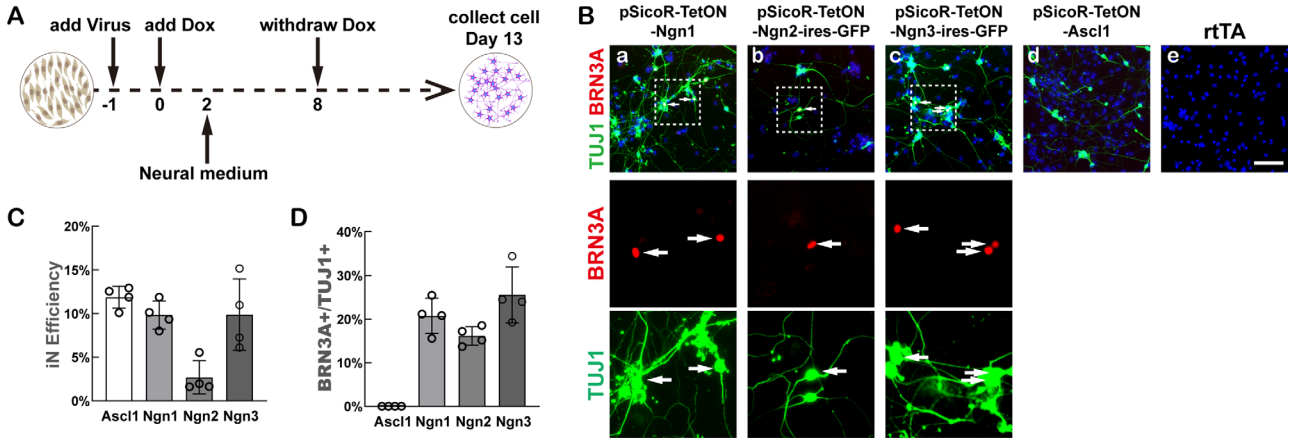

Figure 1. Single Ngn family TFs are sufficient to induce BRN3A$^+$-iNs from MEFs. (**A**) A diagram illustrating the experimental scheme. (**B**) Immunofluorescent images showing TUJ1 (*green*) and BRN3A (*red*) expression in each group of cells. Areas squared by *dotted lines* are shown in higher magnification in separate channels to highlight the BRN3A$^+$;TUJ1$^+$ cells. *White arrows* point to the BRN3A$^+$;TUJ1$^+$ cells. *Scale bar*: 100 µm. (**C**) Quantification of the TUJ1$^+$-iN induction efficiency by different TFs. (**D**) Quantification of the percentage of BRN3A$^+$ versus TUJ1$^+$ cells in iNs induced by different TFs. Data in **C** and **D** are represented as the means ± standard deviations.

The iN induction efficiencies of *Ngn1* and *Ngn3* were 9.84% ± 1.62% and 9.88% ± 4.06%, respectively, slightly lower than that of *Ascl1* (11.87% ± 1.26%), while the iN induction efficiency of *Ngn2* was only 2.67% ± 1.92% (Fig. 1C). Thus, *Ngn1* and *Ngn3* were more potent than *Ngn2* in reprogramming MEFs into iNs. Interestingly, we found that in all three Ngn-overexpressing groups, some of the TUJ1$^+$ cells also expressed BRN3A (Fig. 1Ba–c), suggesting that Ngns alone were able to induce a putative RGC-like cell fate. In contrast, no BRN3A$^+$ cells were observed in the *Ascl1*-overexpressing group (Fig. 1B-d), which is consistent with our previous report.[10] Quantification of the percentage of TUJ1$^+$-iNs that expressed BRN3A showed that 20.75% ± 4.40% of *Ngn1*-iNs, 16.14% ± 2.14% of *Ngn2*-iNs, and 25.54% ± 6.38% of *Ngn3*-iNs expressed BRN3A (Fig. 1D). Thus, these results demonstrated that Ngn-TFs are able to work alone to convert MEFs into BRN3A$^+$ putative RGC-like neurons. Ngn-TF–induced iNs survived well during the reprogramming process as demonstrated by TUNEL assays (Supplementary Fig. S2). Among the three family members, *Ngn1* and *Ngn3* are more efficient than *Ngn2* in reprogramming MEFs into iNs. We thus focused on *Ngn1* and *Ngn3* in our subsequent studies.

Prolonged Ngn Overexpression Promotes BRN3A$^+$-iN Reprogramming Efficiency

We next wanted to test whether better induction outcomes can be achieved through prolonged Ngn overexpression. We thus prolonged the Dox treatment time from 7 days in our initial test to periods between 7 and 28 days and collected the cells at the end of Dox treatment. Quantification of the TUJ1$^+$ and BRN3A$^+$ cells showed that, within 14 days, prolonged Dox treatment continued to increase both the percentage of TUJ1$^+$ cells and the percentage of BRN3A$^+$/TUJ1$^+$ cells. The percentage of TUJ1$^+$ cells increased from 8.72% ± 1.05% after 7 days of *Ngn1* overexpression to 19.00% ± 3.93% after 14 days of *Ngn1* overexpression, while the percentage of the BRN3A$^+$/TUJ1$^+$ population increased from 22.55% ± 2.83% after 7 days of *Ngn1* overexpression to 50.50% ± 2.54% after 14 days of *Ngn1* overexpression (Fig. 2A). However, beyond 14 days, further extending the *Ngn1* overexpression time did not further increase the reprogramming efficiency; instead, further prolonged overexpression beyond 14 days even decreased the reprogramming efficiency (Fig. 2A). The Dox treatment window test showed that 14 days was also the best overexpression time for *Ngn3*-mediated BRN3A$^+$-iN reprogramming (Supplementary Fig. S3A). TUNEL assays suggested that cell death was responsible for the decreased reprogramming efficiency in the prolonged overexpression groups (Supplementary Fig. S3B).

Our previous work showed that FGF2 significantly promoted ABI-mediated iRGC reprogramming. We wondered whether FGF2 would also promote Ngn-mediated BRN3A$^+$-iN reprogramming. We supplemented the culture medium with FGF2 for different durations and examined TUJ1$^+$ and BRN3A$^+$ cells. Quantification showed that continued FGF2 treatment slightly increased the percentage of TUJ1$^+$-iNs, but the beneficial effects reached a plateau at 8 days (Fig. 2B, left). On the other hand, FGF2 treatment had no effect on the percentage of BRN3A$^+$ cells (Fig. 2B, right).

On the basis of these condition tests, we set the Ngn-based iN induction scheme as follows: Ngn expression (Dox treatment) was maintained for 14 days, and FGF2 was added for the first 8 days (Fig. 2C). With this induction scheme, *Ngn1* induced 24.7% ± 3.44% MEFs as TUJ1$^+$-iNs, and 50.7% ± 1.25% of them were BRN3A$^+$, while *Ngn3* induced 21.90% ± 8.45% MEFs as TUJ1$^+$-iNs, and 51.13% ± 9.19% of them were BRN3A$^+$. The induced iN fate was stable, as continued cultures of these cells for 2 more weeks still exhibited healthy neuron morphology and TUJ1 and BRN3A expression (Fig. 2D). We costained day 14 cells with TUJ1, BRN3A, and GFP (cells were infected with *pSicoR-TetON-Ngn1-ires-GFP*, *pSicoR-TetON-Ngn2-ires-GFP*, *pSicoR-TetON-Ngn3-ires-GFP* lentiviruses), and the results showed that all TUJ1$^+$ cells and TUJ1$^+$;BRN3A$^+$ cells were GFP$^+$, suggesting that the reprogramming effects were cell autonomous (Supplementary Fig. S4).

Ngn-Reprogrammed iNs Resemble RGCs at the Transcriptome Level

To characterize Ngn-iNs at the transcriptome level, we transfected MEFs with *pSicoR-TetON-Ngn1-ires-GFP* or *pSicoR-*

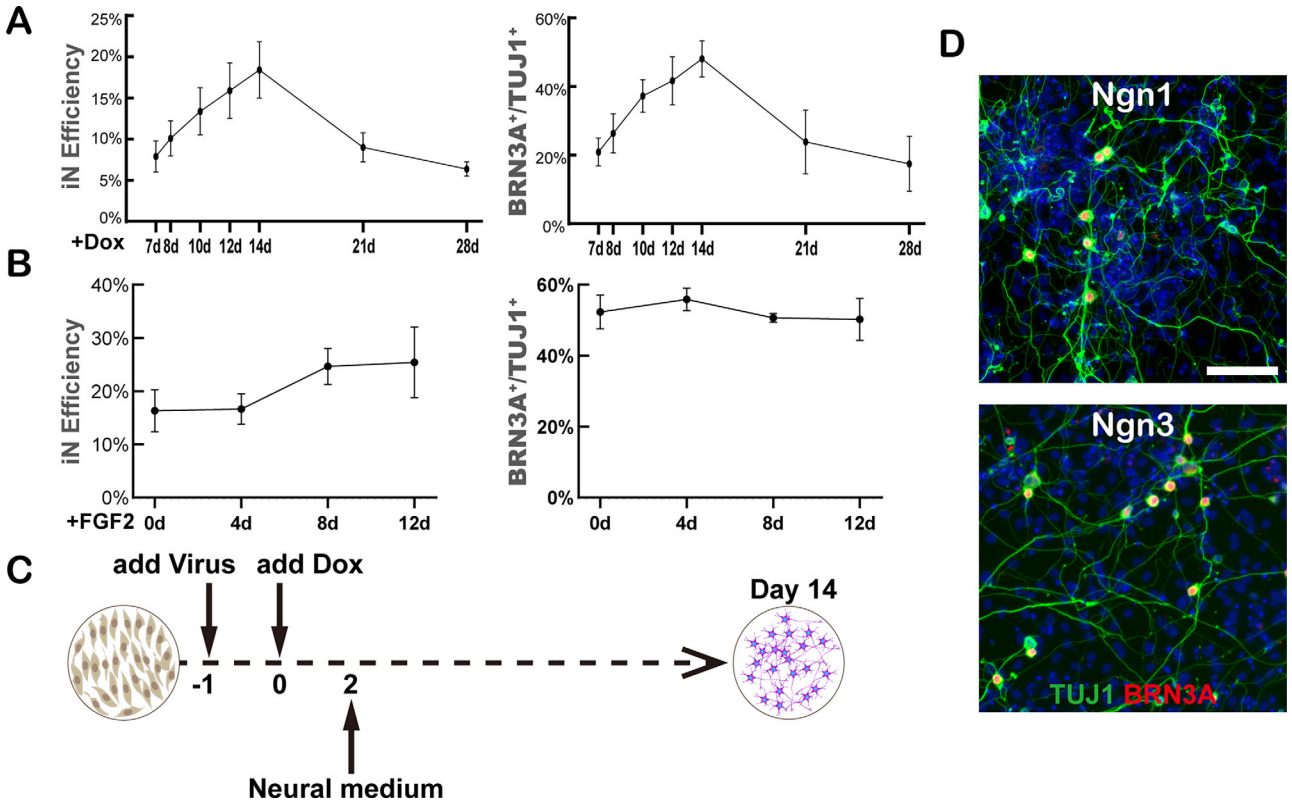

Figure 2. Optimization of the Ngn-based BRN3A$^+$-iN induction scheme. (**A**) Quantification of iN induction efficiency and percentage of BRN3A$^+$ versus TUJ1$^+$ cells induced by different *pSicoR-TetON-Ngn1* overexpression (Dox treatment) times. (**B**) Quantification of iN induction efficiency and percentage of BRN3A$^+$ versus TUJ1$^+$ cells induced by 14 days of *pSicoR-TetON-Ngn1* overexpression with different FGF2 treatment times. (**C**) The final Ngn-based BRN3A$^+$-iN induction scheme. (**D**) Immunofluorescent images showing TUJ1 (*green*) and BRN3A (*red*) expression of *Ngn1*- and *Ngn3*-induced iNs. MEFs were infected with *pSicoR-TetON-Ngn1* or *pSicoR-TetON-Ngn3* lentiviruses and induced with Dox for 14 days, and cells were cultured for 7 more days and collected. *Scale bar*: 100 µm.

TetON-Ngn3-ires-GFP and used FACS to sort GFP$^+$ cells 14 days after Dox induction. We then performed RNA-seq on sorted cells. The sample correlation analyses showed that the transcriptomes of cells induced by *Ngn1* or *Ngn3* for 14 days were dramatically different from those of the original MEFs (Fig. 3A). On the other hand, the transcriptomes of *Ngn1*-induced cells and those of *Ngn3*-induced cells were intermingled together in the heatmap (Fig. 3A), suggesting that iNs induced by *Ngn1* and those induced by *Ngn3* were very similar to each other. We then performed DEG analyses to identify genes dramatically upregulated or downregulated in *Ngn1/3*-induced iNs compared with original MEFs. The DEG analyses showed that 4558 genes and 4334 genes were significantly upregulated in *Ngn1*-iNs and *Ngn3*-iNs, respectively, while 3180 genes and 3182 genes were significantly downregulated in *Ngn1*-iNs and *Ngn3*-iNs, respectively, compared with MEFs (Figs. 3B, 3C). However, when comparing the transcriptomes of *Ngn1*-iNs and *Ngn3*-iNs, only 57 genes were differentially expressed between the two groups of cells (Fig. 3D), again demonstrating that iNs induced by *Ngn1* and *Ngn3* were very similar to each other.

We next performed GO term enrichment analyses on DEGs to examine what cellular processes were activated or repressed in *Ngn1/3*-induced iNs. GO terms representing essential neuronal functions, such as "axonogenesis" and "synapse organization," were significantly enriched in the transcriptome of *Ngn*-iNs (Fig. 3E), while GO terms related to MEF activity, such as "regulation of mitotic cell cycle" and "wound healing," were significantly enriched in DEGs downregulated in the transcriptome of *Ngn*-iNs (Fig. 3F). We then performed GSEA on all genes to further reveal GO terms activated or repressed in *Ngn*-iNs versus original MEFs. The results further supported the conclusion that *Ngn1/Ngn3* reprogrammed MEFs toward neuronal fate. In particular, GSEA showed that RGC-related pathways, such as "neural retina development" and "retinal ganglion cell axon guidance," were significantly more active in *Ngn*-iNs than in MEFs, while "positive regulation of fibroblast proliferation" and "positive regulation of cell cycle process" were significantly more active in MEFs than in *Ngn*-iNs (Figs. 3G, 3H). We next examined the expression patterns of a list of RGC-specific marker genes[10,20] in *Ngn*-iNs. The results showed that RGC-specific genes were upregulated in *Ngn1/3*-iNs (Fig. 3I). The upregulated genes include key RGC development regulators such as *Pou4f1*, *Atoh7*, *Neurod2*, and *Pax6*. Among them, *Pax6* has been shown to be a unique marker for RGCs to distinguish them from other peripheral sensory neurons,[21] and the expression of *Atoh7*, which is well known for its roles in promoting the fate of RGCs, is also relatively restricted to the retina.[22–25] RGCs share many molecular signatures with peripheral sensory neurons, including BRN3A expression. We examined the expression of *Runx1* and *Runx3*, two key cell fate regulators for dorsal root ganglion sensory neurons.[26] The results showed that they were absent from Ngn-iNs. Thus, the expression of RGC-specific

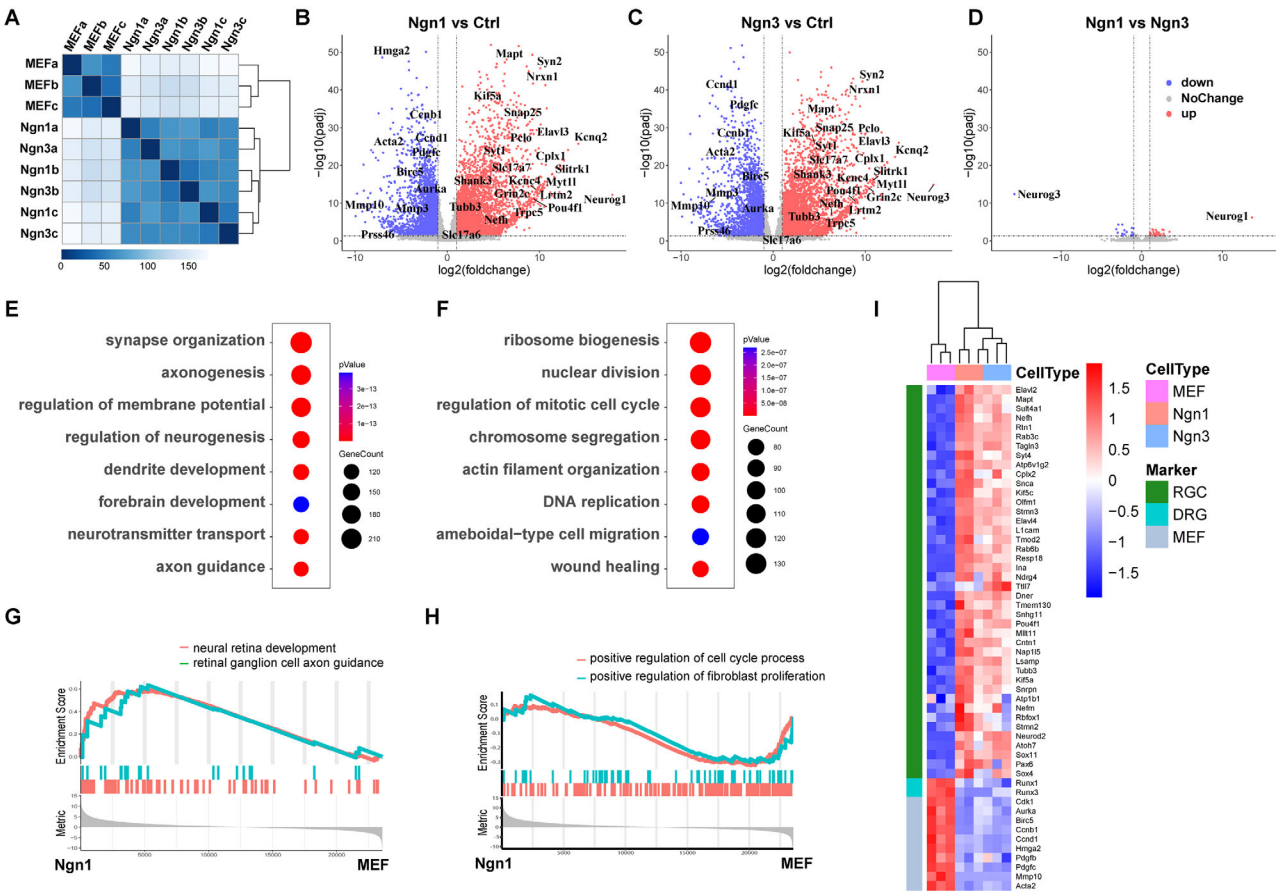

Figure 3. *Ngn*-iNs resemble RGCs at the transcriptome level. (**A**) A heatmap showing the degree of similarity between different samples. *Ngn1* and *Ngn3* groups of samples were FACS-sorted GFP$^+$ cells from MEFs infected with *pSicoR-TetON-Ngn1-ires-GFP* and *pSicoR-TetON-Ngn3-ires-GFP*, respectively. (**B**) A volcano plot showing gene expression differences between *Ngn1*-iN and control MEFs (infected with rtTA lentiviruses). (**C**) A volcano plot showing gene expression differences between *Ngn3*-iN and control MEFs. (**D**) A volcano plot showing gene expression differences between *Ngn1*-iNs and *Ngn3*-iNs. (**E**) A bubble plot showing GO terms enriched in the genes upregulated in *Ngn1*-iNs compared with control MEFs. (**F**) A bubble plot showing GO terms enriched in the genes downregulated in *Ngn1*-iNs compared with control MEFs. (**G**) A GSEA plot showing GO terms upregulated in *Ngn1*-iNs. (**H**) A GSEA plot showing GO terms downregulated in *Ngn1*-iNs. (**I**) A heatmap showing the expression patterns of RGC marker genes, dorsal root ganglion marker genes, and MEF marker genes in different groups of cells.

genes and absence of peripheral sensory neuron genes indicate that iNs induced by *Ngn1/3* are biased toward RGC fate. In addition, genes important for the maturation and projection neuron function of RGCs, including those regulating axon/dendrite development and organization (*Mapt*, *Nefh*, *Kif5a*), synapse organization (*Slitrk1*, *Lrtm2*, *Nrxn1*, *Pclo*, *Shank3*), neurotransmitter transport (*Syt1*, *Cplx1*, *Syn2*, *Snap25*, *Slc17a7*), and generation of neural membrane potential (*Kcnq2*, *Kcnc4*, *Trpc5*, *Grin2c*, *Cacng2*), were dramatically upregulated in Ngn-induced iNs (Figs. 3B, 3C, 3I). Taken together, the transcriptome examination demonstrated that the neuronal fate of *Ngn1/3*-iNs was biased toward a functional RGC-like neuron state.

Ngn-Induced RGC-Like iNs Are Functional Neurons and Capable of Engaging in Synaptic Communication With Native Retinal Neurons

RNA-seq analyses showed that *Ngn1/3*-induced RGC-like iNs expressed a series of genes essential for the electrophysiologic activities of mature neurons, including essential synaptic component genes, such as *Pclo*, *Shank3*, *Syn1* (*Synapsin I*), *Syn2* (*Synapsin II*), *Syp*, and *Syt1*; ion channels that regulate membrane potential, such as *Kcnq2*, *Kcnc4*, *Trpc5*, *Grin2c*, and *Cacng2*; and glutamate transporters, including *Slc17a7* (*vGlut1*) and *Slc17a6* (*vGlut2*) (Figs. 3B, 3C, 3E, 3I). Immunofluorescence staining further confirmed that *Ngn1/3*-induced TUJ1$^+$-iNs expressed SYNAPSIN (*Syn1/2*) and vGLUT1 (*Slc17a7*) (Fig. 4A). To directly test the electrophysiologic functions of *Ngn1/3*-induced RGC-like iNs, we performed patch-clamp experiments. The results showed that all examined *Ngn1*-iNs and *Ngn3*-iNs exhibited depolarized resting membrane potentials, averaging –69.07 ± 3.67 mV and –68.80 ± 4.09 mV, respectively (Fig. 4B). Under voltage-clamp mode, all examined *Ngn1*-iNs (n = 11) and *Ngn3*-iNs (n = 18) exhibited fast inward currents followed by outward currents (Fig. 4C, left), suggesting active voltage-gated Na$^+$ and K$^+$ channel activities. Under current-clamp mode, all examined *Ngn1*-iNs (n = 11) and *Ngn3*-iNs (n = 18) fired action potentials, and most of them fired repetitive action potentials (Fig. 4C, right). Next, we wanted to test whether *Ngn*-induced RGC-like neurons can form functional synaptic connections with retinal neurons. For this purpose, we plated *Ngn1-ires-GFP*–induced iNs on top of the preprepared p7 mouse retinal neurons and cocultured them. After 7 days of cocul-

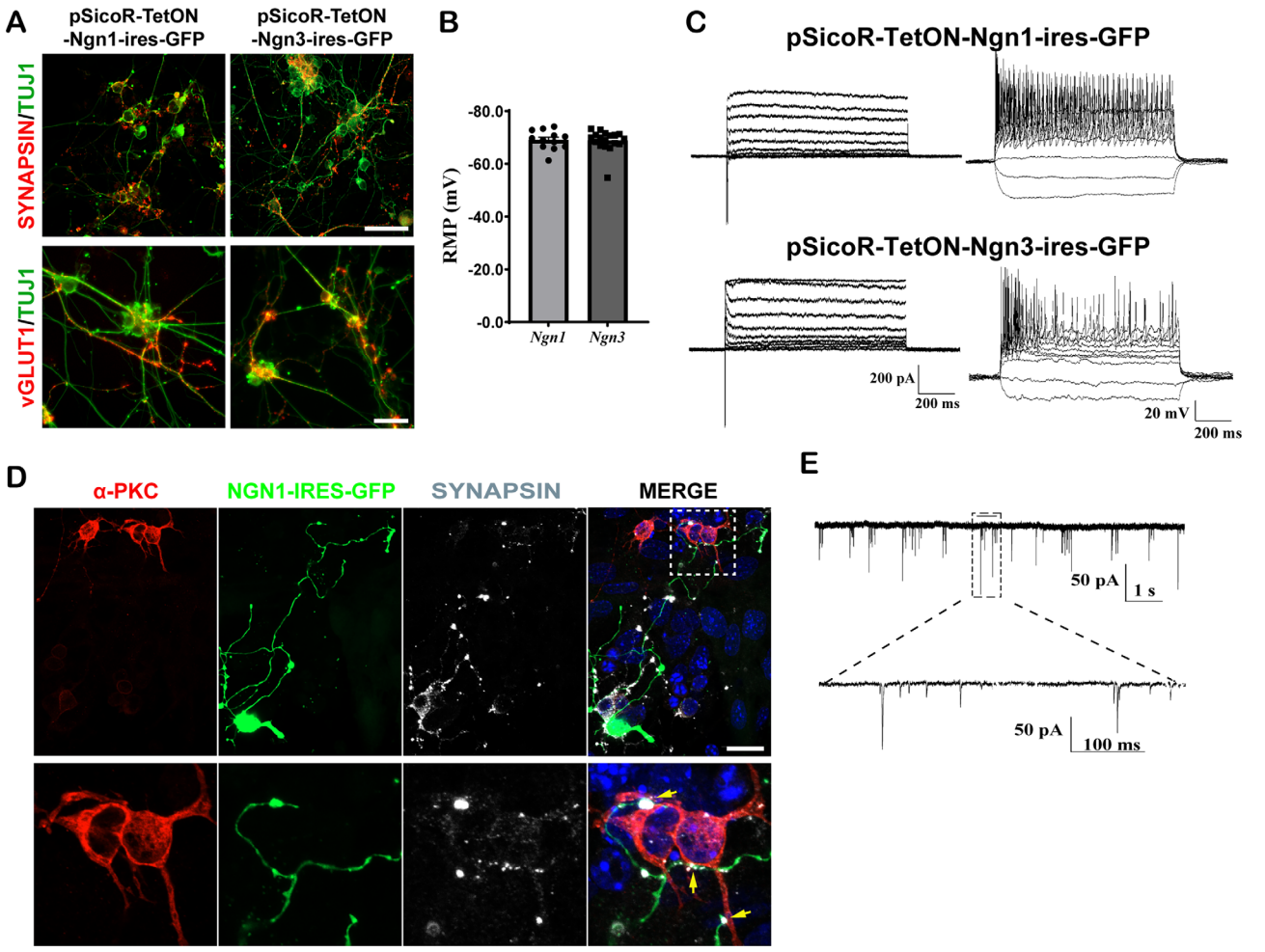

Figure 4. *Ngn*-iNs exhibit functional RGC electrophysiology. (**A**) Immunofluorescent images showing SYNAPSIN and vGLUT1 expression in *Ngn1*- and *Ngn3*-iNs. *Scale bars*: 50 µm. MEFs were infected with *pSicoR-TetON-Ngn1-ires-GFP* or *pSicoR-TetON-Ngn3-ires-GFP*. (**B**) Quantification of the resting membrane potential (RMP) of *Ngn1*- and *Ngn3*-iNs. MEFs were infected with *pSicoR-TetON-Ngn1-ires-GFP* or *pSicoR-TetON-Ngn3-ires-GFP*. (**C**) *Left*: under voltage-clamp mode, *Ngn1*- and *Ngn3*-iNs exhibited fast inward Na^+ currents and outward K^+ currents. *Right*: under current-clamp mode, *Ngn1*- and *Ngn3*-iNs fired repetitive action potentials. MEFs were infected with *pSicoR-TetON-Ngn1-ires-GFP* or *pSicoR-TetON-Ngn3-ires-GFP*. (**D**) A confocal image showing that a GFP^+ *Ngn1*-iN forms synaptic connections with α-PKC^+ native retinal bipolar cells. Cells squared by *dotted lines* are shown at higher magnification. *Yellow arrows* point to the $SYNAPSIN^+$ synaptic connections. *Scale bar*: 20 µm. (**E**) *Ngn1*-iNs exhibited postsynaptic currents when cocultured with native retinal neurons. MEFs were infected with *pSicoR-TetON-Ngn1-ires-GFP*.

ture, we found that GFP^+ *Ngn1*-iNs formed $SYNAPSIN^+$-synaptic connections with α-PKC^+–native retinal bipolar cells (Fig. 4D, yellow arrows). We then used patch clamp to measure the postsynaptic membrane activities of GFP^+ *Ngn1*-iNs. We detected that 3 out of 10 cells exhibited postsynaptic currents (PSCs) (Fig. 4E), demonstrating the synaptic communication competence of *Ngn1*-iNs with native retinal neurons. Taken together, these electrophysiologic examinations demonstrated that *Ngn*-induced iNs are functional mature neurons and capable of engaging in synaptic communications with native retinal neurons.

Ngn1 and *Ngn3* Activate Neuron and RGC Developmental Genes Early During Reprogramming

To reveal the possible direct events that *Ngn*-TFs elicited in MEFs early during reprogramming, we performed RNA-seq on MEFs 24 hours after *Ngn1/3* overexpression. Interestingly, 24 hours of *Ngn1* or *Ngn3* overexpression was sufficient to significantly modify the transcriptome of MEFs (Fig. 5A). Twenty-four hours of *Ngn1* overexpression caused 982 genes to be significantly upregulated and 929 genes to be significantly downregulated (Fig. 5B), while 24 hours of *Ngn3* overexpression caused 1014 genes to be significantly upregulated and 975 genes to be significantly downregulated (Fig. 5C). In contrast, the transcriptomes of MEFs overexpressing *Ngn1* and those overexpressing *Ngn3* were very similar to each other (Fig. 5D), again demonstrating the interchangeable function of *Ngn1* and *Ngn3* in regulating gene expression in MEFs. GO term enrichment analyses showed that 24 hours of *Ngn1/3* overexpression induced the expression of many genes that are important for neuron development, maturation, or function, such as those involved in "ion transmembrane transport," "neurogenesis," and "forebrain development" (Figs. 5E, 5F). Interestingly, the expression of many genes that are essential for RGC development,

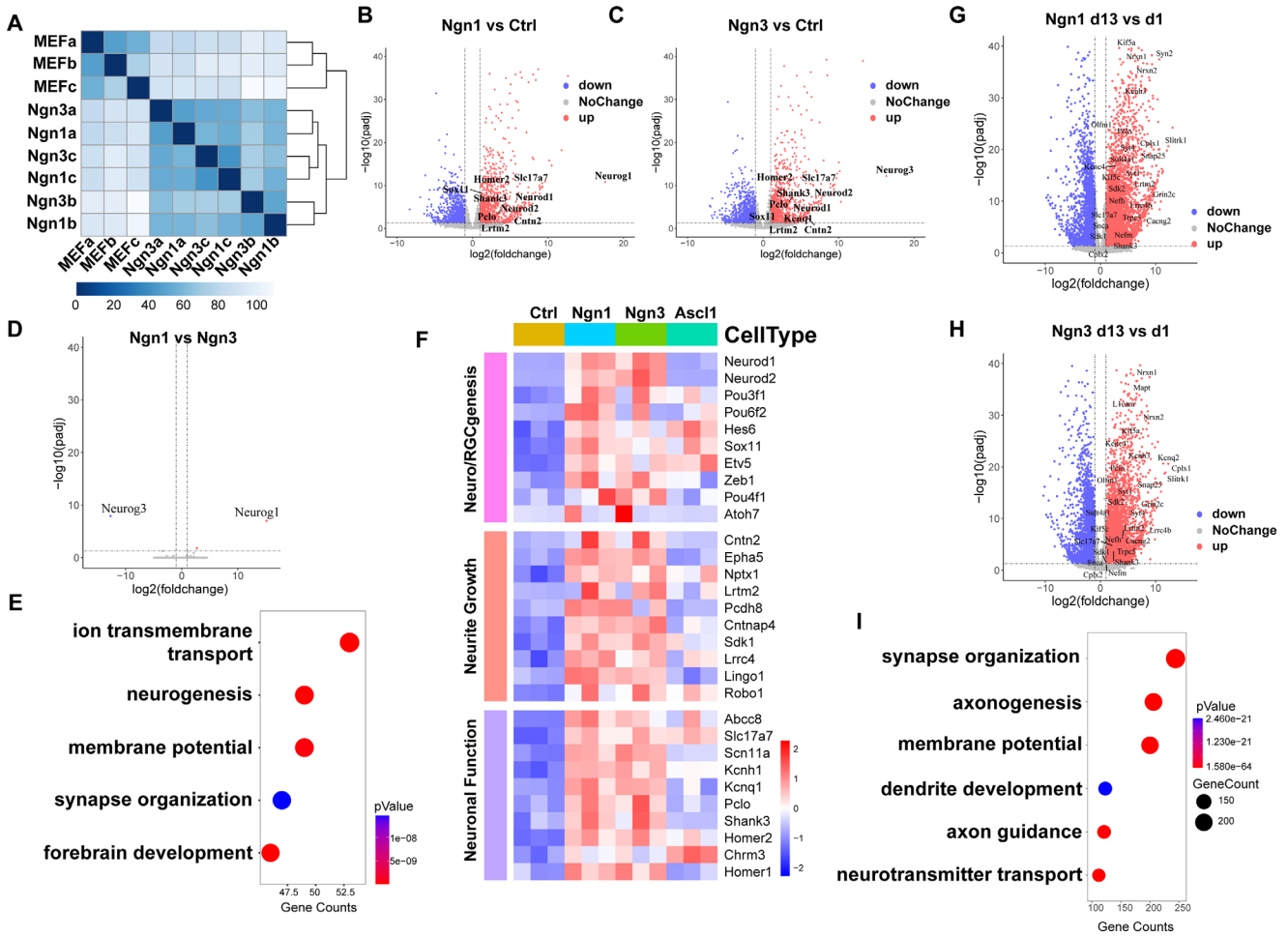

Figure 5. Transcriptome changes in MEFs induced by 24 hours of *Ngn1* or *Ngn3* overexpression. (**A**) A heatmap showing the degree of similarity between different samples. *Ngn1* and *Ngn3* groups of samples were FACS-sorted GFP^{+} cells from MEFs infected with *pSicoR-TetON-Ngn1-ires-GFP* and *pSicoR-TetON-Ngn3-ires-GFP*, respectively. (**B**) A volcano plot showing gene expression differences between MEFs overexpressing *Ngn1* for 24 hours and control MEFs. (**C**) A volcano plot showing gene expression differences between MEFs overexpressing *Ngn3* for 24 hours and control MEFs. (**D**) A volcano plot showing gene expression differences between MEFs overexpressing *Ngn1* and MEFs overexpressing Ngn3 for 24 hours. (**E**) A bubble plot showing GO terms enriched in the genes upregulated in *Ngn1*-overexpressing MEFs compared with control MEFs. (**F**) A heatmap showing that 24 hours of *Ngn1* or *Ngn3* overexpression elicited the expression of many neurogenic or RGCgenic genes and other neuronal development and functional genes. Gene expression pattern of MEFs overexpressing Ascl1 for 24 hours was shown for comparison. (**G**) A volcano plot showing gene expression differences between MEFs overexpressing *Ngn1* for 24 hours and 13 days. (**H**) A volcano plot showing gene expression differences between MEFs overexpressing *Ngn3* for 24 hours and 13 days. (**I**) A bubble plot showing GO terms enriched in the genes upregulated in cells overexpressing *Ngn1* for 13 days compared with cells overexpressing *Ngn1* for 24 hours.

such as *Neurod2*, *Pou6f2*, *Sox11*, *Pou4f1*, and *Atoh7*, was already upregulated by 24 hours of *Ngn1/3* overexpression (Fig. 5F). On the other hand, *Ascl1* failed to stimulate the expression of these genes (Fig. 5F), which explains why *Ascl1* alone failed to induce RGC-like neuron fate. We next compared the transcriptomes of cells induced by *Ngn1/Ngn3* for 14 days with those induced for 24 hours. The comparison showed that genes that are involved in biological processes that are essential for the maturation and electrophysiologic function of neurons, such as synapse organization (*Slitrk1*, *Slitrk3*, *Lrtm2*, *Nrxn1*, *Nrxn2*, *Pclo*, *Shank3*, *Lrrc4b*, *Sdk1*, *Sdk2*), axon/dendrite development and organization (*Nefm*, *Nefb*, *Kif5a*, *Kif5c*, *Olfm1*), regulation of membrane potential (*Kcnq2*, *Kcnc4*, *Kcnh3*, *Kcna1*, *Trpc5*, *Grin2c*, *Cacng2*), and neurotransmitter transport (*Syt4*, *Cplx2*, *Snca*, *Cplx1*, *Syt1*, *Syn2*, *Snap25*, *Syp*, *Slc17a7*), were significantly upregulated in day 14 *Ngn1/3*-induced cells relative to day 1–induced cells, suggesting that *Ngn1* and *Ngn3* continue to reprogram the transcriptome of MEFs toward mature neuron status (Figs. 5G–I). Thus, the RNA-seq analyses of the transcriptome changes elicited by 24 hours of *Ngn1/3* overexpression demonstrated that these two *Ngn*-TFs possess potent RGC-like neuron fate induction capacity.

Ngn1 and *Ngn3* Induced Late-Stage RPCs to Generate RGCs In Vivo

Encouraged by the potent RGC-like neuron fate induction capacity exhibited by *Ngn1/3* on MEFs in vitro, we wondered whether *Ngn1/3* can induce RGCs through reprogramming in vivo. We chose late-stage RPCs to test this possibility. During mouse retinal development, RGCs are generated by early RPCs during embryonic days 11 to 18. After

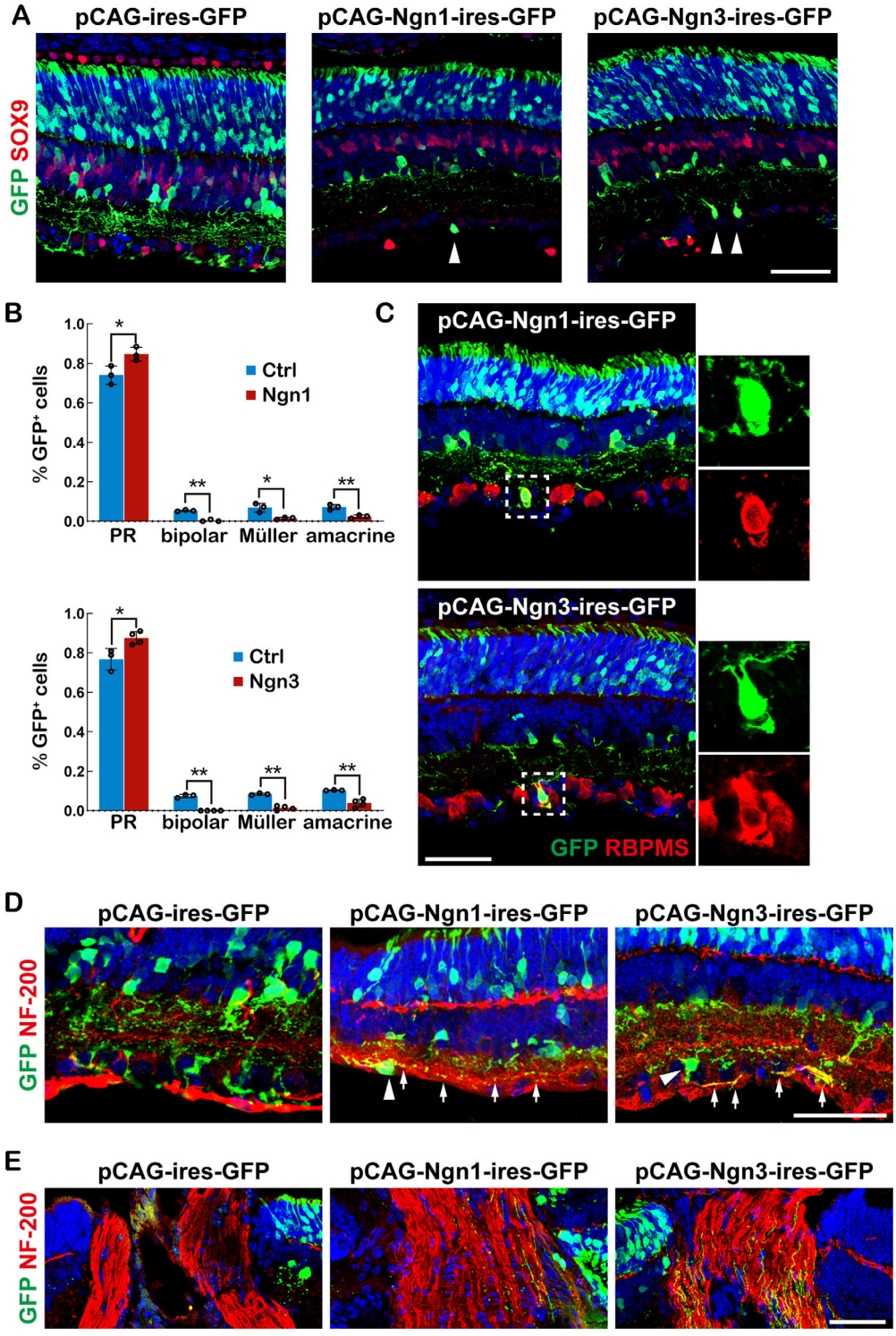

Figure 6. *Ngn1* or *Ngn3* reprograms late-stage RPCs to generate RGCs. (**A**) Confocal images of p14 retinas stained for GFP and SOX9. The retinas were transfected with plasmids overexpressing *Ngn1* or *Ngn3* or empty vector via in vivo electroporation at p1. *White arrowheads* point to GFP$^+$ cells in the RGC layer. (**B**) Quantification of the cell compositions of GFP-labeled electroporated cells. The data are represented as the means ± standard deviations. $^{**}P < 0.01$. (**C**) Confocal images illustrating the GFP$^+$ cells in the RGC layer express RBPMS. The GFP$^+$;RBPMS$^+$ cells squared with *dotted lines* are shown at higher magnification in separate channels on the right. (**D**) Confocal images illustrating the GFP$^+$ cells in the RGC layer extend long axons and are positive for RGC axon marker NF200. *White arrowheads* point to GFP$^+$ cells in the RGC layer, and *white arrows* point to GFP$^+$;NF200$^+$ axons. (**E**) Confocal images showing that the optic discs of the eyes electroporated with *Ngn1*- or *Ngn3*-overexpressing plasmids contain many GFP$^+$;NF200$^+$ axons. *Scale bars*: 50 µm.

Investigative Ophthalmology & Visual Science

birth, late-stage RPCs in the retina lack the competence to generate RGCs and only give rise to amacrine cells, rods, bipolar cells, and Müller glial cells.[27] We used a mouse pup retina in vivo electroporation technique to introduce *Ngn1*- and *Ngn3*-overexpressing plasmids (*pCAG-Ngn1-ires-GFP* and *pCAG-Ngn3-ires-GFP*) into late-stage RPCs of postnatal day 1 (p1) pups (Supplementary Fig. S5) and traced the cell-type composition of the progenies of electroporated RPCs at p14. The results showed that in the *Ngn1* and *Ngn3* overexpression groups, significantly more photoreceptor cells were generated at the expense of Müller glial cells, bipolar cells, and amacrine cells (Figs. 6A, 6B and Supplementary Fig. S6), suggesting that *Ngn1* and *Ngn3* changed the differentiation activity of late-stage RPCs. More excitingly, we occasionally observed GFP^+ cells with typical RGC morphology on the surface layer of the retinas electroporated with *Ngn1* or *Ngn3* overexpression plasmids, which were never observed in the control retinas (Fig. 6A, white arrowheads), indicating that *Ngn1/3* induced some late-stage RPCs to differentiate into RGCs. RGC marker staining showed that these retinal surface layer–located GFP^+ cells were positive for RBPMS (Fig. 6C), demonstrating the RGC identity of these cells. However, none of these GFP^+ cells were positive for BRN3A (Supplementary Fig. S7), suggesting that these induced RGCs were of $BRN3A^-$ subtype RGCs. Because the appearance of GFP^+ cells in the RGC layer of *Ngn1*- or *Ngn3*-overexpressing retinas was a rare event, quantifying the efficiency of RGC fate induction by *Ngn1/3* in vivo is not practical. Nonetheless, from zero to the appearance of RGCs is a significant change to demonstrate the ability of Ngns to induce an RGC fate in vivo. Moreover, some of the GFP^+ cells in the RGC layer were observed to extend long $NF200^+$ axons traveling in the nerve fiber layer (Fig. 6D, white arrows). Most interestingly, we observed abundant GFP^+;$NF200^+$ axons extending toward and through the optic discs in the eyes electroporated with *Ngn1* or *Ngn3* overexpression plasmids, which were never observed in the control eyes (Fig. 6E), further demonstrating that RGCs were generated by late-stage RPCs overexpressing *Ngn1* or *Ngn3*. Thus, mouse pup retina in vivo electroporation experiments demonstrated that *Ngn1* and *Ngn3* can reprogram late-stage RPCs to change their developmental competence to generate RGCs in vivo.

Discussion

RGCs or RGC-like cells generated in culture dishes are valuable cellular sources for RGC biology research and glaucoma translational study purposes and thus have been explored widely in the field. RGCs can be obtained through directed differentiation of pluripotent stem cells; however, such methods often require a lengthy culture time. Overexpressing RGC fate-promoting TFs can significantly accelerate this process. It has been shown that by overexpressing *Atoh7*, RGC-like cells can be generated from mouse induced pluripotent stem cells (iPSCs).[28] Because *Ngn2* has been shown to drive the initiation of the RGC generation wavefront during retinal development,[29] it has often been selected to test its ability to induce RGC fate. Indeed, it has been shown that overexpressing *Ngn2* could induce RGC-like cells from human pluripotent stem cells in as short as 6 days.[30] The shortcoming of using pluripotent stem cells as the starting cells for RGC generation is that it requires considerable efforts and care to prepare pluripotent stem cells and concerns regarding leftover PSCs. Direct somatic cell reprogramming provides an alternative strategy to generate RGCs in culture dishes. Previously, we showed that fibroblasts can be efficiently reprogrammed into RGC-like neurons by a combination of three TFs, *Ascl1*, *Brn3b*, and *Islet1* (ABI), in vitro. However, any single TF of this TF cocktail is incompetent to induce an RGC-like fate or even a generic neuronal fate.[10] In this study, we found that a single TF of any member of the Ngn family was capable of inducing RGC-like functional neurons, although the induction efficiency of *Ngn2* was much lower than that of the other two family members. Previously, Meng et al.[31] showed that, in combination with *Ascl1* and *Brn3b*, *Ngn2* can reprogram MEFs into RGC-like neurons; however, *Ngn2* alone was unable to induce neuron fate from MEFs, different from what was found in this study. The inability of *Ngn2* alone to induce neuron/RGC fate from MEFs in Meng et al.[31] might be due to insufficient *Ngn2* overexpression in their in vitro reprogramming system. Ngn family TFs are known to promote neurogenesis in retinas and dorsal root ganglia.[29,32] Exploiting the potent neurogenetic potential of Ngns, they have been used to induce peripheral sensory neurons from MEFs; however, additional TFs, such as *Brn3a*, *Brn3b*, *Ascl1*, *Isl2*, and *Klf7*, are needed to accomplish this task.[17,33] In this study, we show that when overexpressed alone, *Ngn1/2/3* reprograms MEFs into iNs biased toward an RGC-like neuron fate. These Ngn-induced iNs expressed a group of RGC-specific genes, such as *Atoh7* and *Pax6*, but did not express genes that are essential for peripheral sensory neuron development. It appears that, compared to peripheral sensory neuron fate, RGC fate is relatively easier to induce from MEFs. How do Ngns direct iNs toward a fate biased toward RGC? This might be due to the ability of Ngns to induce the upregulation of *Atoh7* and *Pax6* in MEFs. *Atoh7* is relatively specifically expressed in the retina and is essential for RGC genesis, maturation, and survival.[22,24,25] Ngns have been shown to be able to directly bind to the promoter region of Atoh7 and promote its expression.[34] In the future, it will be worth performing immunostaining experiments to confirm and examine the expression dynamics of PAX6 and ATOH7 during the Ngn-induced RGC-like fate reprogramming processes. It will also be interesting to measure the direct genomic targets of Ngn-TFs and the epigenetic changes upon Ngn-TF overexpression. Such studies would reveal whether Ngn-TFs directly upregulate *Atoh7* expression in MEFs. Such studies would also reveal whether Ngn-TFs function as pioneer factors to drive MEF-to-RGC fate reprogramming. The protocol developed in this study provides an alternative and simpler method than the ABI-based methods we established previously to induce RGC-like neurons in vitro, which are valuable cellular sources for in vitro glaucoma translational studies. On the other hand, the RGC-like cell induction efficiency by *Ngn1* and *Ngn3* was only slightly over 10%, much lower than the 42% efficiency achieved by the ABI-induction method. Combining Ngn-TFs with other TFs or supplementing with small molecules might improve the Ngn-TF–based RGC-like neuron induction efficiency and is worth future tests.

In this study, we found that late-stage RPCs overexpressing *Ngn1* or *Ngn3* generated more rods at the expense of all other types of retinal cells normally generated at the time in *Ngn1/3*-overexpressing retinas, a phenotype reminiscent of what happens when Notch signaling is inhibited,[35,36] suggesting that *Ngn1/3* overexpression might promote RPCs to exit the cell cycle and generate retinal neurons normally produced at the time. Most interestingly, we found that *Ngn1*

Investigative Ophthalmology & Visual Science

and *Ngn3* are capable of inducing RGC fate in vivo, a phenotype that cannot simply be explained by a general neural induction function of Ngns. During development, all retinal neurons are generated by RPCs in a sequential manner, which continue to adjust their competent states to generate different types of retinal cells in different stages of retinal development. The changes in the competent states are accompanied by changes in the RPC transcriptome and epigenome so that early-stage RPCs and late-stage RPCs are distinct from each other.[37,38] RGCs are the first type of retinal cells generated by early-stage RPCs in all vertebrates studied. In mice, RGCs are generated by early RPCs during embryonic days 11 to 18.[27] When performing retinal in vivo electroporation on p1 mouse pups, only the progenies of late-stage RPCs (including rods, bipolar cells, amacrine cells, and Müller glial cells) are labeled at p14, while RGCs are absent, because the plasmids can access only proliferation-active late-stage RPCs in this method.[39] The appearance of RGCs in the progenies of *Ngn1/3*-overexpressing late-stage RPCs suggests that *Ngn1* and *Ngn3* reprogrammed late-stage RPCs to obtain certain differentiation competence features of early-stage RPCs. Although *Ngn1* and *Ngn3* are not expressed in the developing retina, *Ngn2* has been shown to be expressed by embryonic early-stage RPCs and plays important roles in initiating the retinogenesis wavefront,[29] suggesting that Ngn-TFs are potent in wiring the gene regulatory network controlling early retinogenesis. The exact cellular and molecular events elicited by *Ngn1/3* in postnatal late RPCs are worth future further investigation. Recently, great progress has been made in reprogramming Müller glial cells to regenerate retinal neurons in situ in the adult mouse retina. However, the regeneration potential of Müller cells seems to be biased toward bipolar and amacrine interneurons or photoreceptors.[7–9] A more recent report has shown that Müller cells overexpressing the ABI-TF combination show signs of RGC-like fate induction. However, the in vivo–induced RGC-like fate seems rudimentary.[11] As the last cell type generated by late-stage RPCs, Müller glial cells share many gene expression profile similarities with late-stage RPCs.[38,40–42] Our finding that Ngn-TFs can reprogram late-stage RPCs to generate RGCs is exciting. In the future, it will be interesting to explore the ability of Ngn-TFs to reprogram Müller glial cells in adult retinas.

Acknowledgments

The authors thank the staff of the Laboratory Animal Center at the State Key Laboratory of Ophthalmology, Zhongshan Ophthalmic Center, for technical support.

Supported by Guangzhou Municipal Science and Technology (2023A03J0190), the National Natural Science Foundation of China (82060176, 81870659), and the Natural Science Foundation of Hainan Province (822MS190).

Disclosure: **K. Zhang**, None; **W. Cai**, None; **Y. Xin**, None; **Q. He**, None; **C. Chen**, None; **M. Zeng**, None; **S. Chen**, None

References

1. Weinreb RN, Aung T, Medeiros FA. The pathophysiology and treatment of glaucoma: a review. *JAMA*. 2014;311:1901–1911.
2. Jonas JB, Aung T, Bourne RR, et al. Glaucoma. *Lancet*. 2017;390:2183–2193.
3. Tham YC, Li X, Wong TY, et al. Global prevalence of glaucoma and projections of glaucoma burden through 2040: a systematic review and meta-analysis. *Ophthalmology*. 2014;121:2081–2090.
4. Morris SA, Daley GQ. A blueprint for engineering cell fate: current technologies to reprogram cell identity. *Cell Res*. 2013;23:33–48.
5. Wang H, Yang Y, Liu J, Qian L. Direct cell reprogramming: approaches, mechanisms and progress. *Nat Rev Mol Cell Biol*. 2021;22:410–424.
6. Xu J, Du Y, Deng H. Direct lineage reprogramming: strategies, mechanisms, and applications. *Cell Stem Cell*. 2015;16:119–134.
7. Jorstad NL, Wilken MS, Grimes WN, et al. Stimulation of functional neuronal regeneration from Muller glia in adult mice. *Nature*. 2017;548:103–107.
8. Yao K, Qiu S, Wang YV, et al. Restoration of vision after de novo genesis of rod photoreceptors in mammalian retinas. *Nature*. 2018;560:484–488.
9. Hoang T, Wang J, Boyd P, et al. Gene regulatory networks controlling vertebrate retinal regeneration. *Science*. 2020;370:eabb8598.
10. Wang J, He Q, Zhang K, et al. Quick commitment and efficient reprogramming route of direct induction of retinal ganglion cell-like neurons. *Stem Cell Reports*. 2020;15:1–16.
11. Todd L, Jenkins W, Finkbeiner C, et al. Reprogramming Muller glia to regenerate ganglion-like cells in adult mouse retina with developmental transcription factors. *Sci Adv*. 2022;8:eabq7219.
12. Wapinski OL, Vierbuchen T, Qu K, et al. Hierarchical mechanisms for direct reprogramming of fibroblasts to neurons. *Cell*. 2013;155:621–635.
13. Brzezinski JAT, Kim EJ, Johnson JE, Reh TA. Ascl1 expression defines a subpopulation of lineage-restricted progenitors in the mammalian retina. *Development*. 2011;138:3519–3531.
14. Ma W, Wang SZ. The final fates of neurogenin2-expressing cells include all major neuron types in the mouse retina. *Mol Cell Neurosci*. 2006;31:463–469.
15. Bertrand N, Castro DS, Guillemot F. Proneural genes and the specification of neural cell types. *Nat Rev Neurosci*. 2002;3:517–530.
16. Tsunemoto R, Lee S, Szucs A, et al. Diverse reprogramming codes for neuronal identity. *Nature*. 2018;557:375–380.
17. Blanchard JW, Eade KT, Szucs A, et al. Selective conversion of fibroblasts into peripheral sensory neurons. *Nat Neurosci*. 2015;18:25–35.
18. Matsuda T, Cepko CL. Controlled expression of transgenes introduced by in vivo electroporation. *Proc Natl Acad Sci USA*. 2007;104:1027–1032.
19. Badea TC, Cahill H, Ecker J, et al. Distinct roles of transcription factors brn3a and brn3b in controlling the development, morphology, and function of retinal ganglion cells. *Neuron*. 2009;61:852–864.
20. Macosko EZ, Basu A, Satija R, et al. Highly parallel genome-wide expression profiling of individual cells using nanoliter droplets. *Cell*. 2015;161:1202–1214.
21. Xiao D, Deng Q, Guo Y, et al. Generation of self-organized sensory ganglion organoids and retinal ganglion cells from fibroblasts. *Sci Adv*. 2020;6:eaaz5858.
22. Brown NL, Kanekar S, Vetter ML, et al. Math5 encodes a murine basic helix-loop-helix transcription factor expressed during early stages of retinal neurogenesis. *Development*. 1998;125:4821–4833.
23. Mao CA, Cho JH, Wang J, et al. Reprogramming amacrine and photoreceptor progenitors into retinal ganglion cells by replacing Neurod1 with Atoh7. *Development*. 2013;140:541–551.

24. Yang Z, Ding K, Pan L, et al. Math5 determines the competence state of retinal ganglion cell progenitors. *Dev Biol*. 2003;264:240–254.
25. Wang SW, Kim BS, Ding K, et al. Requirement for math5 in the development of retinal ganglion cells. *Genes Dev*. 2001;15:24–29.
26. Marmigere F, Ernfors P. Specification and connectivity of neuronal subtypes in the sensory lineage. *Nat Rev Neurosci*. 2007;8:114–127.
27. Cepko CL, Austin CP, Yang X, et al. Cell fate determination in the vertebrate retina. *Proc Natl Acad Sci USA*. 1996;93:589–595.
28. Chen M, Chen Q, Sun X, et al. Generation of retinal ganglion-like cells from reprogrammed mouse fibroblasts. *Invest Ophthalmol Vis Sci*. 2010;51:5970–5978.
29. Hufnagel RB, Le TT, Riesenberg AL, Brown NL. Neurog2 controls the leading edge of neurogenesis in the mammalian retina. *Dev Biol*. 2010;340:490–503.
30. Luo Z, Chang KC, Wu S, et al. Directly induced human retinal ganglion cells mimic fetal RGCs and are neuroprotective after transplantation in vivo. *Stem Cell Reports*. 2022;17:2690–2703.
31. Meng F, Wang X, Gu P, et al. Induction of retinal ganglion-like cells from fibroblasts by adenoviral gene delivery. *Neuroscience*. 2013;250:381–393.
32. Ma Q, Fode C, Guillemot F, Anderson DJ. Neurogenin1 and neurogenin2 control two distinct waves of neurogenesis in developing dorsal root ganglia. *Genes Dev*. 1999;13:1717–1728.
33. Wainger BJ, Buttermore ED, Oliveira JT, et al. Modeling pain in vitro using nociceptor neurons reprogrammed from fibroblasts. *Nat Neurosci*. 2015;18:17–24.
34. Matter-Sadzinski L, Matter JM, Ong MT, et al. Specification of neurotransmitter receptor identity in developing retina: the chick ATH5 promoter integrates the positive and negative effects of several bHLH proteins. *Development*. 2001;128:217–231.
35. Jadhav AP, Mason HA, Cepko CL. Notch 1 inhibits photoreceptor production in the developing mammalian retina. *Development*. 2006;133:913–923.
36. Mizeracka K, DeMaso CR, Cepko CL. Notch1 is required in newly postmitotic cells to inhibit the rod photoreceptor fate. *Development*. 2013;140:3188–3197.
37. Lyu P, Hoang T, Santiago CP, et al. Gene regulatory networks controlling temporal patterning, neurogenesis, and cell-fate specification in mammalian retina. *Cell Rep*. 2021;37:109994.
38. Clark BS, Stein-O'Brien GL, Shiau F, et al. Single-cell RNA-seq analysis of retinal development identifies NFI factors as regulating mitotic exit and late-born cell specification. *Neuron*. 2019;102:1111–1126.e5.
39. Matsuda T, Cepko CL. Electroporation and RNA interference in the rodent retina in vivo and in vitro. *Proc Natl Acad Sci USA*. 2004;101:16–22.
40. Nelson BR, Ueki Y, Reardon S, et al. Genome-wide analysis of Muller glial differentiation reveals a requirement for Notch signaling in postmitotic cells to maintain the glial fate. *PLoS One*. 2011;6:e22817.
41. Blackshaw S, Harpavat S, Trimarchi J, et al. Genomic analysis of mouse retinal development. *PLoS Biol*. 2004;2:E247.
42. Roesch K, Jadhav AP, Trimarchi JM, et al. The transcriptome of retinal Muller glial cells. *J Comp Neurol*. 2008;509:225–238.

Investigative Ophthalmology & Visual Science